CALPHAD: Computer Coupling of Phase Diagrams and Thermochemistry 73 (2021) 102259

Contents lists available at ScienceDirect

Calphad

journal homepage: http://www.elsevier.com/locate/calphad

Melting temperature prediction by thermoelastic instability: An *ab initio* modelling, for periclase (MgO)

Marcello Merli [a,*], Alessandro Pavese [b]

[a] Department of Earth and Sea Sciences (DiSTeM), University of Palermo, Via Archirafi 36, 90123, Palermo, Italy
[b] Earth Sciences Department – University of Turin, Via Valperga Caluso 35, 10100, Turin, Italy

ARTICLE INFO

Keywords:
Melting temperature
Thermo-elastic instability
Catastrophe theory
Ab-initio modelling
Periclase (MgO)

ABSTRACT

Melting temperature (T_M) is a crucial physical property of solids and plays an important role for the characterization of materials, allowing us to understand their behavior at non-ambient conditions. The present investigation aims i) to provide a physically sound basis to the estimation of T_M through a "critical temperature" (T_C), which signals the onset of thermodynamic instability due to a change of the isothermal bulk modulus from positive to negative at a given P_C-V_C-T_C point, such that $(\partial P/\partial V)_{VC,TC} = -(\partial^2 F/\partial V^2)_{VC,TC} = 0$; ii) to discuss the case of periclase (MgO), for which accurate melting temperature observations as a function of pressure are available. Using first principles calculations, quasi-harmonic approximation and anharmonic correction, we model the Helmholtz potential, *i.e.* $F(V,T)$, and determine pressure thereby. A comparison between measured and predicted T_M values as a function of pressure shows achievement of an average discrepancy of ~2.9%, in the range 0–25 GPa and 3000–5000 K.

1. Introduction

The melting temperature (T_M) of a solid is a fundamental physical property, which plays a relevant role in developing phase diagrams, understanding the behavior of many materials at non-ambient conditions and designing possible applications. In particular, we are interested in minerals that are involved in natural reactions occurring at high-pressure and high-temperature conditions. In this view, we focus on solids with a crystal structure, and henceforth we shall use the term "solids" to mean "crystal solids". Notwithstanding the vastly recognized relevance of predicting T_Ms, melting temperature modelling still remains a challenging task [1].

The main difficulty lies in the intrinsic complexity to model melts' Gibbs energy, on the one hand, and in the non-trivial definition of a reliable phenomenological principle underlying the change of state from solid to liquid, on the other hand.

Several authors have proposed principles that underpin the collapse of a crystal, thereby developing approaches that relate melting to the appearance of particular trends, which involve one or more macroscopic, or microscopic, observables of the solid phase.

Lindemann [2] hypothesized melting to occur when neighboring atoms' oscillations around average positions become larger than inter-atomic distances. Such a principle was revised by Gilvarry [3], who adapted it to the case of the atomic vibrations inferred from the Debye-Waller factors measured in diffraction experiments. Ross [4] generalized the Lindemnn melting law by elucidating its links to statistical mechanics; Kuramoto [5], recalling the Ross's principle, reformulated the theory of melting using statistical thermodynamics and seeking conditions of equilibrium between solid and melt by modelling their partition functions.

Stacey and Irvine [6] derived an equation for melting from the Clausius-Clapeyron relationship, thus providing a general thermodynamic basis to the phenomenological Lindemann's law.

Herzfeld and Goeppert Mayer [7] related the occurrence of melting to thermo-elastic anomalies revealed by the appearance of a minimum in the P–V curve. Born [8] generalized the correlation between breakdown of a crystal and its elastic behavior, associating melting with the occurrence of elastic shear modulus tending to zero. Ida [9] and Boyer [10] contributed to shedding light on the mechanisms underlying the change of state from solid to liquid and produced two papers that share the same title: "Theory of melting based on lattice instability". The former discussed the role of anharmonic effects in causing breakdown of a crystal. The latter provided a thorough survey about the relation between melting and thermo-elastic instability, gathering into a coherent

* Corresponding author.
E-mail address: marcello.merli@unipa.it (M. Merli).

https://doi.org/10.1016/j.calphad.2021.102259
Received 14 October 2020; Received in revised form 11 February 2021; Accepted 13 February 2021

synthesis the contributions of earlier authors who shared the opinion that the change of state from solid to liquid is to be associated with the occurrence of anomalies affecting the *P–V* curve. In particular, Boyer [10] described the equation of state of a solid in terms of

$$P(V,T) = P_{st}(V) + P_{th}(V,T)$$

Where the subscripts *st* ("static") and *th* ("thermal") account for contributions to pressure from lattice + zero-point energy (independent of *T*) and vibrational energy (dependent on *T*), respectively. If at a "critical" temperature, T_C, there occurs that P_{st} (V_C,T_C) = -P_{th}(V_C,T_C), then the solid undergoes thermo-elastic instability, which is a prologue to a breakdown of the system.

The occurrence of thermo-elastic instability as a sign heralding a change of state has recently been re-examined by Owens [11] in the case of alkali halides, using the Debye approximation. The cross-over temperature between P_{st} and P_{th} has been interpreted by the quoted author as an approximation of T_M that is underestimated by about 6% with respect to the observations. Digilov and Abramovich [12], coupling the Debye model with statistical thermodynamics, were able to correlate the appearance of thermo-elastic instability to a "critical" value of the thermal pressure, *i.e.* $P_{th} = K_0\,(e\delta)^{-1}$, where K_0 and δ are bulk modulus at 0 K and Grüneisen parameter, respectively.

In this light, the present work aims to discuss the relation between melting temperature as a function of pressure, $T_M(P)$, and the appearance of thermodynamic instability, caused by the violation of fundamental relationships involving thermodynamic potentials. In particular, we focus on the *P–V-T* (pressure-temperature-volume) equilibrium surface, whose *P* is obtained by the Helmholtz potential as a function of *V* and *T*, to estimate $T_M(P)$ *via* a "critical temperature", $T_C(P)$. The latter will be introduced in the ensuing section and portends the occurrence of instability, a prologue to the breakdown of the crystal structure. We model the thermodynamic potentials using *ab-initio* calculations, quasi-harmonic lattice dynamics and an anharmonic correction. We compare the obtained results with experimental data, in the case of MgO (periclase). The choice of such a mineral was dictated by the following reasons: i) comparatively simple structure, which allows us to focus on methodological aspects; ii) amply investigated and measured $T_M(P)$ curve, which makes it possible to reliably compare predictions with experimental results; iii) relevance of MgO in providing a structure model, of interest both to Earth Sciences and Material Sciences. Previous investigations about MgO melting are reported by Refs. [13,14], who used molecular dynamics and semi-empirical potentials to model T_M, and by Ref. [15], who employed molecular dynamics in combination with DFT-theory to reproduce the melting slope.

2. Theoretical

2.1. Thermodynamic instability

Let a system be at equilibrium with a thermo-barostat, at *P-T*. We split the system into two sub-systems [16], whose volumes (V_1 and V_2) and entropies (S_1 and S_2) are such that $V_1 = V \times \xi$, $V_2 = V \times (1\text{-}\xi)$ and $S_1 = S \times \xi$, $S_2 = S \times (1\text{-}\xi)$, $0 \le \xi \le 1$. We shift one sub-system off equilibrium with respect to the other, in terms of $V_1 = V/2 + \delta V$ *versus* $V_2 = V/2$ - δV, and $T_1 = T + \delta T$ *versus* $T_2 = T\text{-}\delta T$, thus preserving the total volume and temperature, *i.e.*

$$\delta V_{total} = \delta V_1 + \delta V_2 = 0 \tag{1.a}$$

$$\delta T_{total} = \delta T_1 + \delta T_2 = 0. \tag{1.b}$$

Using $F_1(V_1,T_1)$, $F_2(V_2,T_2)$ and $F(T,V)$ to address the Helmholtz energy of either sub-system and of the total system, respectively, one has that

$$\left(\frac{\partial^2 F_1}{\partial V_1 \partial T_1}\right)_{V_1=V\times\xi,T_1=T} = \left(\frac{\partial^2 F_2}{\partial V_2 \partial T_2}\right)_{V_2=V\times(1-\xi),T_2=T} = \left(\frac{\partial^2 F}{\partial V \partial T}\right), \tag{2.a}$$

$$\frac{1}{\xi}\left(\frac{\partial^2 F_1}{\partial T_1^2}\right)_{V_1=V\times\xi,T_1=T} = \frac{1}{(1-\xi)}\left(\frac{\partial^2 F_2}{\partial T_2^2}\right)_{V_2=V\times(1-\xi),T_2=T} = \left(\frac{\partial^2 F}{\partial T^2}\right), \tag{2.b}$$

$$\xi\left(\frac{\partial^2 F_1}{\partial V_1^2}\right)_{V_1=V\times\xi,T_1=T} = (1-\xi)\left(\frac{\partial^2 F_2}{\partial V_2^2}\right)_{V_2=V\times(1-\xi),T_2=T} = \left(\frac{\partial^2 F}{\partial V^2}\right). \tag{2.c}$$

Moreover, any generic change of a *V-T* system, *i.e.* (V_0,T_0)→(V_0+ΔV, T_0+ΔT), entails a variation in entropy given by

$$\Delta S = S(V_0+\Delta V, T_0+\Delta T) - S(V_0,T_0) = -\left(\frac{\partial^2 F}{\partial V \partial T}\right)_{V=V_0,T=T_0}\Delta V - \left(\frac{\partial^2 F}{\partial T^2}\right)_{V=V_0,T=T_0}\Delta T. \tag{3.a}$$

If the constraints provided by (1.*a*) and (1.*b*) are fulfilled, then from (3.*a*) it follows that

$$\delta S_{total} = \delta S_1 + \delta S_2 = 0, \tag{3.b}$$

i.e. the entropy of the total system is preserved. In this view, any shift of the two sub-systems, (V_1,T_1,S_1) and (V_2,T_2,S_2), according to (1.*a-b*) leads to an off-equilibrium condition such that the total system evolves towards equilibrium *via* an irreversible transformation driven by a decrease of Helmholtz energy and Internal energy. Let us now focus on the case of the Helmholtz energy and $\xi = 0.5$. Then

$$\delta F_1 = F_1\left(\frac{V}{2}+\delta V, T+\delta T\right) - F_1\left(\frac{V}{2},T\right) \approx \left(\frac{\partial F_1}{\partial T_1}\right)_{V_1=\frac{V}{2},T_1=T}\delta T + \left(\frac{\partial F_1}{\partial V_1}\right)_{V_1=\frac{V}{2},T_1=T}$$
$$\delta V + \frac{1}{2}\left(\frac{\partial^2 F_1}{\partial T_1^2}\right)_{V_1=\frac{V}{2},T_1=T}\delta T^2 + \frac{1}{2}\left(\frac{\partial^2 F_1}{\partial V_1^2}\right)_{V_1=\frac{V}{2},T_1=T}\delta V^2 + \left(\frac{\partial^2 U_1}{\partial T \partial V_1}\right)_{V_1=\frac{V}{2},T_1=T}$$
$$\delta T \delta V = -\frac{S}{2}\delta T - P\delta V + \frac{1}{4}\left(\frac{\partial^2 F}{\partial T^2}\right)_V \delta T^2 + \frac{1}{4}\left(\frac{\partial^2 F}{\partial V^2}\right)_T \delta V^2 + \left(\frac{\partial^2 F}{\partial T \partial V}\right)_{V,T}\delta T \delta V \tag{4.a}$$

and

$$\delta F_2 = F_2\left(T-\delta T, \frac{V}{2}-\delta V\right) - F_2\left(T,\frac{V}{2}\right) \approx -\left(\frac{\partial F_2}{\partial T_2}\right)_{V_2=\frac{V}{2},T_2=T}\delta T - \left(\frac{\partial F_2}{\partial V_2}\right)_{V_2=\frac{V}{2},T_2=T}$$
$$\delta V + \frac{1}{2}\left(\frac{\partial^2 F_2}{\partial T_2^2}\right)_{V_2=\frac{V}{2},T_2=T}\delta T^2 + \frac{1}{2}\left(\frac{\partial^2 F_2}{\partial V_2^2}\right)_{V_2=\frac{V}{2},T_2=T}\delta V^2 + \left(\frac{\partial^2 F_2}{\partial T_2 \partial V_2}\right)_{V_2=\frac{V}{2},T_2=T}$$
$$\delta T \delta V = +\frac{S}{2}\delta T + P\delta V + \frac{1}{4}\left(\frac{\partial^2 F}{\partial T^2}\right)_V \delta T^2 + \frac{1}{4}\left(\frac{\partial^2 F}{\partial V^2}\right)_T \delta V^2 + \left(\frac{\partial^2 F}{\partial T \partial V}\right)_{V,S}\delta T \delta V \tag{4.b}$$

We sum (4.*a*) and (4.*b*), *i.e.* $\delta F = \delta F_1 + \delta F_2$, and write δF as

$$\delta F = \delta^1 F + \delta^2 F,$$

Where $\delta^1 F$ and $\delta^2 F$ represent the first and second order contributions, respectively, in δT and δV. We readily observe that at

$$\delta^1 F = 0,$$

Whereas

$$\delta^2 F > 0.$$

The second inequality is required for equilibrium to occur at a minimum of *F*, in the case of an irreversible transformation such that $\delta V_{total} = 0$ and $\delta T_{total} = 0$, *i.e.* (1.a) and (1.b).

Hence, $\delta^2 F$ must be a positive definite, homogenous quadratic form in δV and δT [17], *i.e.*

$$\delta^2 F \propto \left(\frac{\partial^2 F}{\partial V^2}\right)_T \delta V^2 + 4\left(\frac{\partial^2 F}{\partial V \partial T}\right)\delta V \delta T + \left(\frac{\partial^2 F}{\partial T^2}\right)_V \delta T^2 > 0. \quad (5)$$

Eq. (5) is associated with the symmetric matrix

$$\boldsymbol{M} = \begin{pmatrix} A & C \\ C & B \end{pmatrix} \quad (6)$$

where $A = (\partial^2 F/\partial V^2)_T$, $B = (\partial^2 F/\partial T^2)_V$, $C = 2\,(\partial^2 F/\partial T \partial V)$. For $\delta^2 F > 0$ to hold, the eigenvalues of the matrix (6), λ_1 and λ_1, must be both positive. Such a requirement implies further restraints in terms of

$$\mathrm{Tr}(\boldsymbol{M}) = \lambda_1 + \lambda_2 > 0 \quad (7.a)$$

and

$$\mathrm{Det}(\boldsymbol{M}) = \lambda_1 \times \lambda_2 > 0. \quad (7.b)$$

Solving the secular equation for the determination of the eigenvalues of matrix (6) and taking into account the restraints of (7.a) and (7.b), one readily finds out a set of inequalities involving *A-B-C* and providing fundamental thermodynamic relationships. Let us leave algebraic details aside and focus our attention on trivial cases only, exploiting the fact that Eq. (5) must hold for any δV and δT value. It follows then:

- $\delta V \neq 0$ and $\delta T = 0$ implies $KT > 0$ (KT = isothermal bulk modulus);
- $\delta V = 0$ and $\delta T \neq 0$ implies $CV/T > 0$ (CV = isochoric specific heat).

The same argument may be used for Internal energy, $U(V,S)$, under an off-equilibrium shift provided by δV and δS. In so doing, we obtain that.

- $\delta V \neq 0$ and $\delta S = 0$ implies $KS > 0$ (KS = adiabatic bulk modulus);
- $\delta V = 0$ and $\delta S \neq 0$ implies $CV > 0$ (CV = isochoric specific heat).

Any change as a function of *P-T* of one of the observables mentioned above (*i.e.* K_S, K_T, C_V; for simplicity, X) from positive to negative, implies a transition from thermodynamic stability to thermodynamic instability. Moreover, there must exist a thermodynamic state, Λ_0, corresponding to "critical" pressure-volume-temperature values, (P_C,V_C,T_C), implying $X(\Lambda_0) = 0$. We chose K_T as thermodynamic key observable to reveal appearance of instability, *i.e.* we seek those *P-T* ranges in which $K_T \leq 0$. We propose to use T_C to *estimate* T_M, in combination with

$K_T > 0$ for $V < V_C$ ($T = T_C$);

$K_T = 0$ for $V = V_C$ ($T = T_C$);

$K_T < 0$ for $V > V_C$ ($T = T_C$).

Fig. 1 visually elucidates this principle in the *P–V* space, at a given temperature. Minima of a *P–V* isotherm depict a phenomenology in which the volume increases, until achievement of a size where the onset of a loss of stability is triggered and the pristine phase cannot exist any longer. This behavior is coherent with the trend commonly exhibited by a solid upon approaching melting in experiments.

Note that due care is required in using T_C as an *estimate* of T_M, at least in two respects: 1) it does not point univocally to a change of state from solid to liquid. For instance, T_C might be related to a pre-melting change of state into a glass [18,19], or to a phase transition [20]; 2) T_C is associated with to the solid phase only, thus expressing its intrinsic instability, and no comparison is made between solid and melt Gibbs energies. All this prompts the need of a careful comparison between predictions and observations to assess the actual efficacy of T_C as an estimate of T_M, and to point out limitations, restrictions and drawbacks of such possible a usage.

A parallelism can be observed between (P_C,V_C,T_C)s and critical points of a crystal electron density, ρ, *i.e.* points at which where $\nabla\rho = 0$. The coalescence of a pair of critical points produces a new critical point, (x_C,

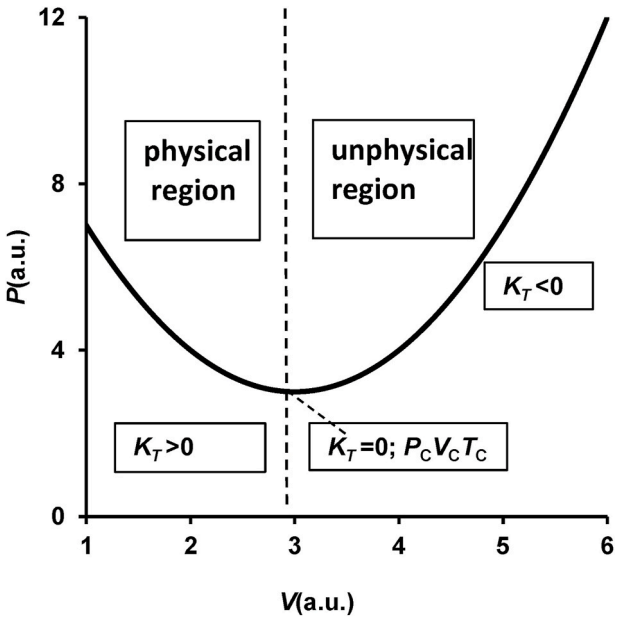

Fig. 1. An example of the critical point topology (P_C-V_C-T_C), in the *P–V* space. Along a given T_C-isotherm, we distinguish two regions: 1) thermodynamic *stability* range, where *P* decreases upon increasing *V* (*i.e.* $K_T > 0$); 2) thermodynamic *instability* range, where *P* increases upon increasing *V* (*i.e.* $K_T > 0$). At P_C-V_C-T_C we have $K_T = 0$; a.u. = arbitrary units.

y_C,z_C), where the ρ′s Hessian matrix is singular, and heralds, by virtue of the catastrophe theory, a transformation to a more stable phase/state [21,22]. The kinship between (P_C,V_C,T_C) and (x_C,y_C,z_C) is disclosed by analyzing the behavior of the Helmholtz function *versus V* around (P_C, V_C,T_C) and observing its analogy to the classical Thom's functions that describe the occurrence of a catastrophe, as shown by Fig. 2, which represents the case of MgO (periclase) before, during and after melting, at *P* = room pressure (here treated as *P* = 0, on account of the low compressibility of MgO). The catastrophe predicted by the Helmholtz

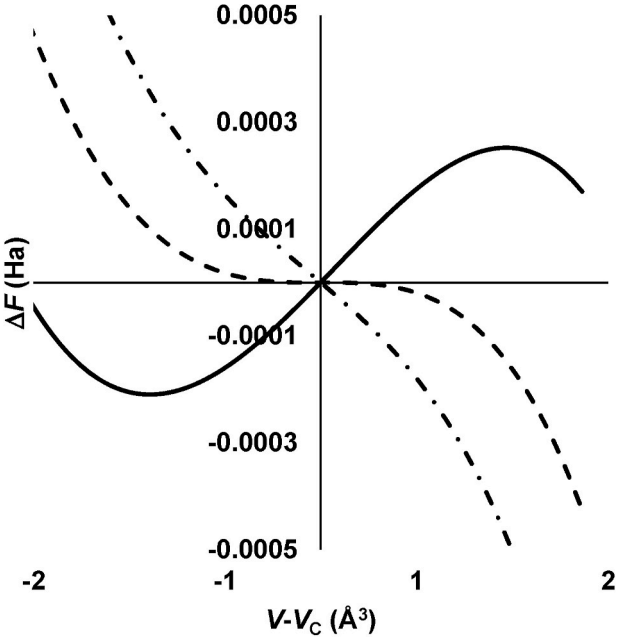

Fig. 2. $F(V,T)$ around V_C at T_C. The trend of a fold-type function, heralding a catastrophe according to the Thom's theory, is displayed. $\Delta F = F(V,T)$-$F(V_C,T)$. Solid line = 2900 K; dashed line = 3114 K; dash-dot line = 3300 K.

energy is of fold-type, *i.e.* reducible to the Thom's function ("unfolding") shown below

$$f(\xi) = 1/3\xi^3 + v\xi \tag{8}$$

Where $f(\xi)$ is the difference between the Helmholtz free energy along the reaction V-path and its value at (P_C = room pressure, V_C,T_C); $\xi = V\text{-}V_C$; v is a control parameter dependent on T. In Fig. 2 the cases (i) $v > 0$ (equivalent to $T < T_C$, $T = 2900$ K, for instance), (ii) $v = 0$ ($T = T_C$, $T_C = 3114$ K, *i.e.* melting temperature predicted by the anharmonic model, see below) and (iii) $v < 0$ (equivalent to $T > T_C$, $T = 3300$ K, for instance) are displayed, respectively. In particular, in the case (i), $f(\xi)$ exhibits two critical points at $V = 21.27$ Å^3 (in the stable region, $V < V_C$) and $V = 23.17$ Å^3 (in the unstable region, $V > V_C$), which have second derivatives of opposite signs. In the case (ii), the two critical points mentioned above coalesce into one at $V_C = 22.18$ Å^3, giving rise to a horizontal inflection (second derivative of *F versus V* equal to zero) at $\xi = 0$, *i.e.* $V = V_C$, that announces MgO melting. In the case (iii), no critical points appear in $f(\xi)$ and the system becomes stable at $P > 1.3$ GPa.

For the sake of completeness, we underscore that full coherence with the Thom's theory is achieved if one uses $F(V,T_C)_{norm}$ in place of $F(V,T_C)$, where the former is defined by

$$F(V,T_C)_{norm} = F(V,T_C) + P_C V,$$

T_C and P_C behaving as control parameters. Note that

$$\left(\frac{\partial F_{norm}}{\partial V}\right)_{V=V_C,T=T_C} = \left(\frac{\partial^2 F_{norm}}{\partial V^2}\right)_{V=V_C,T=T_C} = 0,$$

which does provide the fundamental condition for the occurrence at (P_C, V_C,T_C) of a critical point triggering instability in the context of the catastrophe theory.

2.2. Negative compressibility paradox

Negative *linear* compressibility has long attracted attention [23] and does not violate thermodynamics, as volume reduction takes place in combination with expansion along a given direction [24]. Conversely, negative volume compressibility of an unconstrained solid violates thermodynamic fundamental relationships, indeed, and leads to a behavior against common observations. Let us recall that the definition of the thermal/adiabatic bulk modulus by means of the elastic constant tensor, *i.e.*

$$K_{T,S} = \sum_{j,i=1}^{3} C_{iijj}^{T,S}. \tag{9}$$

$K_{T,S} < 0$ entails that one is able to choose a strain tensor of type (η_1,η_2,η_3,0,0,0) that progressively lowers the deformation energy of a crystal, so that the more deformed the system the more stable it becomes. All this is in conflict with an elastic regime and promotes a plastic-type deformation stabilizing a progressively ever more strained structure.

If we analyze the Gibbs potential of a system as a function of *V-T*, *i.e.* $G(P(V,T),T)$, at isothermal conditions, we have that

$$\frac{\partial G(P(V,T),T)}{\partial V} = \frac{\partial F(V,T)}{\partial V} + \frac{\partial}{\partial V}(PV) = -P + P + V\left(\frac{\partial P}{\partial V}\right)_T = -K_T \tag{10}$$

In the case of an isothermal change from V_0 to V_1, then

$$\Delta G = \int_{V_0}^{V_1} -K_T dV, \tag{11}$$

which, if $K_T < 0$, would entail a decrease of the system's Gibbs energy under a reduction of volume ($V_0 > V_1$). In light of this, such a crystal would monotonically increase its stability with shrinking, notwithstanding overwhelming repulsive forces due to a shortening of the interatomic distances.

2.3. Modelling

We explore the *P–V-T* space by modelling $F(V,T)$, from which we calculate pressure as

$$P = -\left(\frac{\partial F}{\partial V}\right)_T, \tag{12}$$

and determine thereby the instability ranges ($K_T \leq 0$), with the related critical points (P_C,V_C,T_C), whereat

$$\left(\frac{\partial P}{\partial V}\right)_{V_C,T_C} = 0,$$

i.e. $K_T = 0$.

We preliminarily investigated the degree of intrinsic anharmonicity that affects MgO. The exploration of the vibration frequencies as a function of volume did not reveal occurrence of soft-modes, which announce instability driven by a very large anharmonic contribution due to a subset of phonons. Three vibrational modes were studied, at the largest volume explored in the present work, by shifting the atoms according to the related eigenvectors around the equilibrium positions and calculating the resulting lattice energy.

Fig. 3 shows, by way of example, the case of $F1u$ for MgO, at the zone center. The anharmonic contributions become non-negligible for vibrational amplitudes associated with quantum levels of the harmonic oscillator above $\tilde{n}12$. Tests show that the partition function of the related anharmonic oscillator achieves convergence for $n > 50$–60, at temperatures close to those of room pressure melting. All this indicates that we must include somehow anharmonicity in modelling the Helmholtz function.

We used the approach by Oganov and Dorogokupets [25], who express the Helmholtz function as follows:

$$F(V,T) = E_{latt} + F_{QH}(V,T) + \Delta F_A(V,T) \tag{12.a}$$

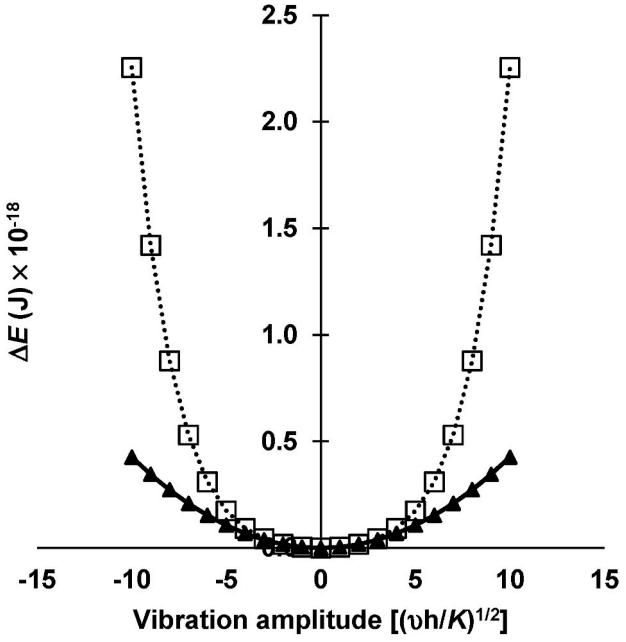

Fig. 3. MgO (periclase). ΔE = lattice energy difference between configurations with atoms shifted according to an eigenvector ($F1u$) from their crystallographic positions and atoms at their crystallographic positions, with respect to the oscillation amplitude. The latter is expressed in $(h\nu/K)^{1/2}$ unit, where ν = harmonic frequency; K = force constant. Squares and dotted line: anharmonic model. Triangles and full line: harmonic model.

where: QH = Quasi Harmonic model, inclusive of the zero-point energy; ΔF_A = anharmonic contribution; E_{latt} = lattice energy. ΔF_A, in turn, is modelled as

$$\Delta F_{th,A} \approx \frac{3}{2} R\, a\, n_{atoms}\, T^2 \tag{12.b}$$

where n_{atoms} is the number of atoms per formula unit, and a is a function of the volume, *i.e.*

$$a(V, V_0) = a_0 \left(\frac{V}{V_0}\right)^m \tag{12.c}$$

where the subscript 0 indicates a reference state (here, V_0 = equilibrium volume at 300 K and room pressure, *i.e.*, V_0 = 18.86 Å^3, by harmonic approximation; $a_0 = 1.427\ 10^{-5}$ K^{-1} and $m = 6.090$; the latter two from Table IV of [25]).

2.4. Computational

Energy of MgO was determined using static and vibrational contributions. The calculations were performed by the CRYSTAL17-code that exploits "Linear Combinations of Atomic Orbitals" [26,27]. We used a hybrid functional, with Hartree-Fock/DFT rate of 0.25, WCGGA exchange functional and LYP correlation functional, following Wu and Cohen [28]. The hybridization rate was chosen to reproduce unit cell volume, bulk modulus and electronic energy gap, at room conditions. The following tolerances that control the accuracy of the self-consistent cycles' integrals were used: 10^{-8} for coulomb overlap; 10^{-8} for coulomb penetration; 10^{-8} for exchange overlap; 10^{-8} for exchange pseudo-overlap in direct space and 10^{-16} for exchange pseudo-overlap in reciprocal space; 10^{-10} a.u. Threshold for SCF-cycles' convergence. The shrinking factors of the reciprocal space (Monkhorst net [29]) and of the secondary reciprocal space net (Gilat net [30]) were set at 6 and 12, respectively. The Mg basis set from Causà et al. [31] was extended by the addition of diffuse *sp* and *d* shells (85-11G* contraction). Oxygen was modelled by means of the O8-411 basis sets of Towler et al. [32,33]. The outer shells' coefficients were optimized by means of the "billy" utility by Towler [34]. The eigenvalue level shifting technique was not used. All the coulomb and exchange bi-electronic integrals have been evaluated exactly (keyword NOBIPOLA). The convergence acceleration method of Anderson [35] was employed. Lattice dynamics calculations were carried out using a 3 × 3 × 3 supercell, which allowed us to sample 27 ***K***-points [36]. The size of the supercell was chosen exploring how it affects specific heat at constant volume (C_V) and entropy (S). In so doing, we observed that passing from 3 × 3 × 3 to 4 × 4 × 4 supercells changes C_V and S within 1%, at room conditions, and within 0.5%, on average in the ranges 0–2000 K. In Fig. 4 the phonon dispersion relations of MgO calculated by CRYSTAL17 (keyword BANDS) and spanning 64 **k**-points along each path in the reciprocal space, are displayed. Such results agree, for instance, with those of https://materialsproject.org/materials/mp-1265/#phonon-dispersion. See Ref. [37], for details about calculations.

The static $E(V)$-curve of MgO was obtained by exploring the V-range [-1.5%,25%], around the room pressure volume. Cell expansion and shrinking are modelled by applying a nominal negative, or positive, pressure, P_{nom}, and modifying then lattice parameters and atomic positions up to achievement of equilibrium between P_{lat} and P_{nom}. In the present case, due to the high-symmetry phase with atoms in special positions, each V-point was modelled by a simple variation of the cell edge. For each V-point, the vibrational energy was determined by combining atomic vibration frequencies of a harmonic model with standard statistical mechanics' formalism, including zero-point vibration. In doing so, we obtained 145 (T,V)-points, and the *ab initio* quasi-harmonic Helmholtz energy was calculated accordingly. $F_{QH}(V,T)$ was then modelled by a V-T expansion, as follows (MATLAB® [38]):

$$F(V,T) = \sum_{j=0}^{n} \sum_{k=0}^{m} p_{j,k} T^j V^k \tag{13}$$

where n and m in our analysis range from 3 up to 5 and m+n ≤ 5. The choice of this interpolation scheme is dictated by merely numerical reasons, provided by: i) achievement of R and $R^2 < 0.9999$, MSSE $<10^{-8}$ and RMSE $<10^{-4}$; ii) t-test statistic of the regression coefficients; iii) convergence of the T and V series. In the present work, we adopted a n = 5 and m = 3 polynomial, thus treating a system with 127 independent "observables", with standardization (by centring and scaling: $<T>\sim1788$ and $\sigma\sim1048$ K, for T; $<V>\sim141.4$ and $\sigma\sim11.28$ Bohr^3, for V) of the dependent variables. The fitting's parameters are reported in Table 1.

To corroborate the validity of the developed model, we compare its predictions with experimental V-T (room pressure), V–P (room temperature) and V–P (along isotherms) curves. In Fig. 5, the equilibrium volumes calculate by F (T,V) are compared with high-temperature experimental data from Ref. [39]: a full agreement is apparent between predictions and measurements.

In Fig. 6 our volume data at 300 and 1100 K are compared with those by Ref. [40], while in Fig. 7 the comparison is between our data at 1000, 2000 and 3000 K and those by Wu [41], over a P-range of 0–40 GPa. Given that such a pressure range is larger than the one we explored, we used an extrapolation of our calculations, which are restricted to 0–7 GPa.

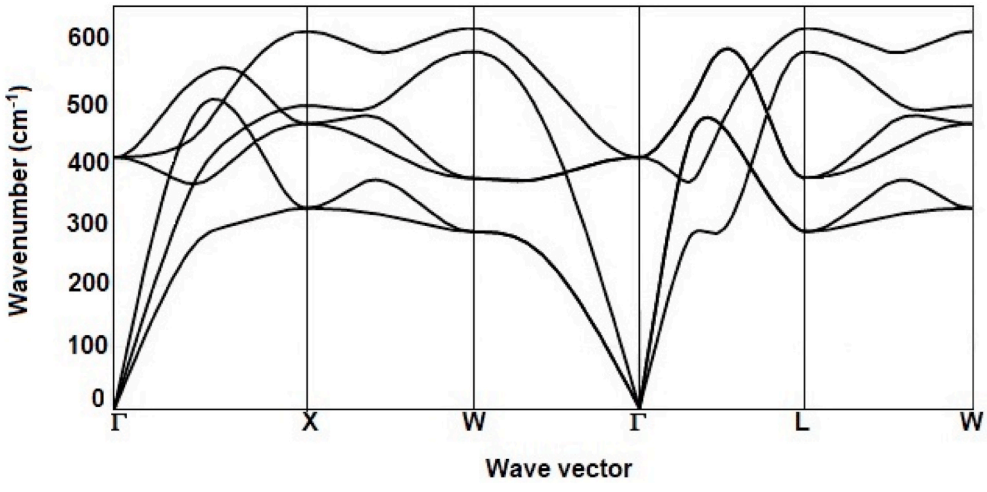

Fig. 4. MgO phonon-dispersion curve.

Table 1
Regression parameters of polynomial fitting of the ab-initio modelled $F_{QH}(T,V)$ and related statistical figures of merit.

Polynomial fit (Eq. (13))		
R	1.0000	
R^2	1.0000	
adjR^2	1.0000	
MSSE	4.1017e-09	
RMSE	6.8433e-05	
SSE	5.9475E-07	
MAE	4.9229e-05	
Parameter	**Value**	**Std. Err.**
p_{00}	−275.20583	7.22E-06
p_{10}	−0.044810989	1.51E-05
p_{01}	0.002323113	1.18E-05
p_{20}	−0.00539901	1.20E-05
p_{11}	−0.00256122	9.97E-06
p_{02}	0.00154408	4.94E-06
p_{30}	0.00094786	1.79E-05
p_{21}	0.00006008	1.38E-05
p_{12}	−0.00010691	8.30E-06
p_{03}	−0.00050399	5.99E-06
p_{40}	−0.00058922	4.44E-06
p_{31}	0.00004876	3.72E-06
p_{22}	0.00001205	3.69E-06
p_{13}	−0.00010252	4.00E-06
p_{50}	0.00022646	5.31E-06
p_{41}	−0.00004114	4.37E-06
p_{32}	−0.00001191	4.26E-06
p_{23}	−0.00000665	4.52E-06

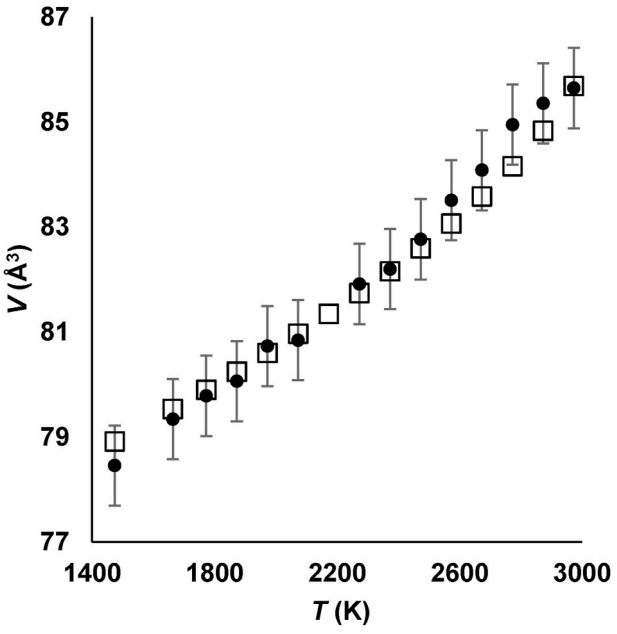

Fig. 5. Comparison between volume values from present work (open squares) and those by Fiquet et al. (1999) [39] (solid circles with experimental error bars).

In the comparisons above, V has been corrected in terms of V_{300}/V_{exp} (see Ref. [41]) where V_{300} is the volume predicted by F_{QH} at $T = 300$ K, whereas V_{exp} is the experimental volume at room conditions. Eventually, for the sake of comparison, we report that at room temperature a F–V interpolation (0–7 GPa) by the second order Birch-Murnghan expansion provides for MgO the following results: $K_0 = 170.7$ GPa and $V_0 = 18.9$ Å^3, to be compared with the following observed figures: $K_0 = 162.8$ GPa [42] and $V_0 = 18.7$ Å^3 [43].

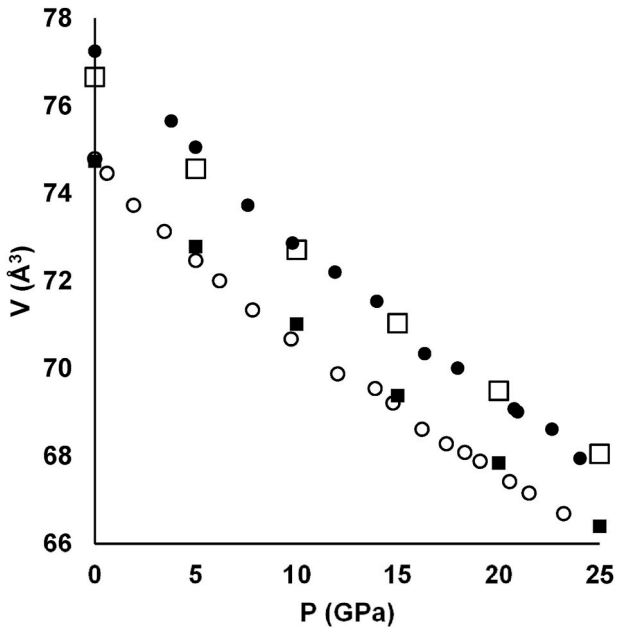

Fig. 6. Comparison between volume data of present work (squares) and those from Fei (1999) [40] (circles). Solid squares = 300 K, open squares = 1100 K; open circles = 300 K, solid circles = 1100 K.

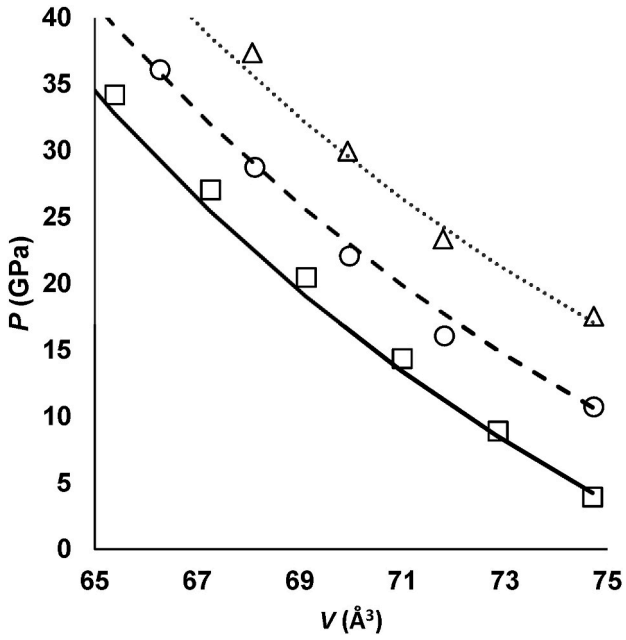

Fig. 7. Comparison between volume data of present work and those from Wu [41] (solid circles). Solid line = data from Wu, 1000 K; dashed line = data from Wu, 2000 K; dash-dotted line = data from Wu, 3000 K; squares = this work, 1000 K; circles = this work, 2000 K; triangles = this work, 3000 K.

3. Results and discussion

In order to determine the melting curve for MgO, we explored the V-T space along isotherms, to find out critical points (P_C,V_C,T_C) at which pressure changes its trend with volume from monotonically decreasing into monotonically increasing, *i.e.* $(\partial^2F/\partial V^2)_{VC,TC} = 0$ at $P_C = -(\partial F/\partial V)_{VC,TC}$.

In Fig. 8, P–V isothermal curves calculated at different temperatures are displayed, by way of example. The location of the related (P_C,V_C,T_C)

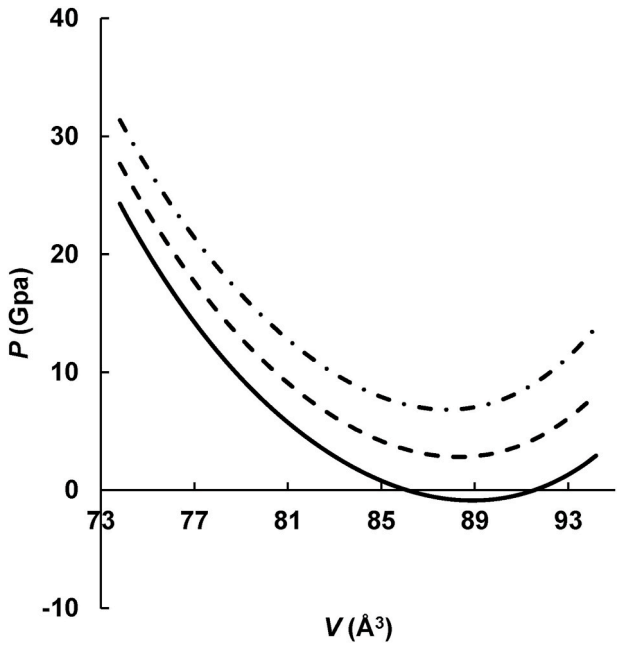

Fig. 8. MgO (periclase). Some isothermal P–V curves that show how we locate the related critical points. Each isotherm provides T_C, and its minimum allows one to determine the critical point. Anharmonic model. Solid line: 3000 K; dashed line: 3500 K; dash-dotted line: 4000 K.

points is provided by the isotherms' minima (see Fig. 1).

The physically sound (P_C,V_C,T_C) points, whereby the melting P-T curve is predicted, are recognized as the "first" critical points found expanding the volume (*i.e.* those with the smallest volume) with respect to its room temperature value (predicted by harmonic calculation), along the isotherm at $T = T_C$ and under the restraints:

$P_C > 0$;

$K_T > 0$ for $V < V_C$;

$K_T = 0$ for $V = V_C$;

$K_T < 0$ for $V > V_C$

Given that from Fig. 1 we have.

i) $(\partial P/\partial V)_T > 0$, $V > V_C$ and $T = T_C$, and
ii) $(\partial P/\partial V)_T < 0$, $V < V_C$ and $T = T_C$,

it follows

$$P(V_C \pm \delta V,T_C) = P_C + \Delta P(V_C \pm \delta V,T_C),$$

Where

$$\Delta P(V_C \pm \delta V,T_C) = P_{lat}(V_C \pm \delta V,T_C) + P_{vib}(V_C \pm \delta V,T_C) - P_C,$$

$\Delta P(V_C \pm \delta V,T_C) \geq 0$,
and, at the critical point, it holds:

$$P_{lat}(V_C,T_C) + P_{vib}(V_C,T_C) = P_C.$$

Melting at ambient pressure requires $P_C = 0$ (we neglect the actual room pressure, as it is irrelevant in the present context), *i.e.*

$$P_{lat}(V_C,T_C) + P_{vib}(V_C,T_C) = 0,$$

corresponding to the very condition posed by Owens [11] and Boyer [10], and that can be fulfilled by virtue of the opposite signs exhibited by the static and thermal pressure components.

Moreover, it is trivial to observe that

$(\partial P_{lat}/\partial V)_T > -(\partial P_{vib}/\partial V)_T$, $V > V_C$ and $T = T_C$,

and

$(\partial P_{lat}/\partial V)_T < -(\partial P_{vib,QH}/\partial V)_T$, $V < V_C$ and $T = T_C$.

Namely, the change of the inequality between the derivatives in volume of static and thermal pressure components underlies the onset of instability.

In Fig. 9, K_T is displayed as a function of P, so that one can easily appreciate the effect of pressure on T_C, under the requirement of having positive pressure values, for the related (P_C,V_C,T_C) point to make physical sense. Note that such K_T values have been determined by Eq. (13), and in this light they are reliable for revealing a change in sign of the bulk modulus (position of the minimum of the P–V curve), rather than for predicting its absolute value (P–V curvature value). For instance, the isotherm at 3000 K yields $K_T = 0$ at a negative pressure value. Such a critical point, which does exist in barely mathematical terms, is not physically acceptable, in keeping with the fact that the system does not melt at 3000 K. Conversely, the isotherm at 3500 K provides $K_T = 0$ at a positive P figure, thus modelling the occurrence of a (P_C-V_C-T_C) point that we can relate to melting, at physically possible conditions.

Fig. 10 illustrates a comparison between the melting P-T curves modelled in the present work (quasi-harmonic and anharmonic models) and experimental data [43,46]. In Table 2, we report the coefficients of two parametrizations of $T_C(P)$, relying on 100 melting points predicted by the anharmonic model up to ~25 GPa, using a 6th order polynomial and the Simon equation.

Extrapolations of the melting temperature to P above those explored by calculations, give results in agreement with observations.

At 135 (about the earth's core-mantle boundary pressure) and 320 GPa (about the supposed pressure in the earth's core) we predict T_C ~ 8050 and ~9750 K, respectively, to be compared with ~7900 and ~9340 K, from experiments [43,47]. Both theoretical curves of Fig. 10 have trends close to one another, with the anharmonic model giving a $T_C(P)$ systematically smaller than the harmonic one of ~2%, on average. Such a difference achieves its maximum at about 2.5 GPa, ~2.5%, and progressively decreases with pressure, thus suggesting that the two

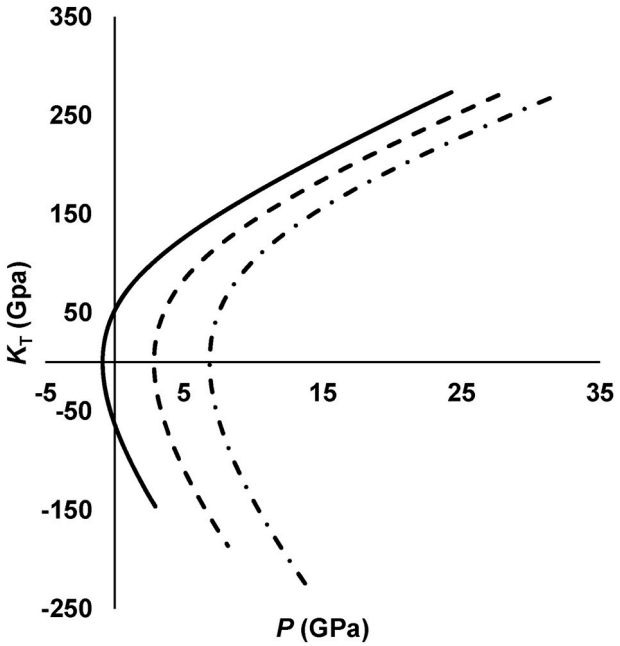

Fig. 9. MgO (periclase). The K_T trend is shown along three isotherms, as a function of pressure. $K_T = 0$ allows one to detect the transition from a stability to instability. $P > 0$ is required to have a physically consistent description. Anharmonic model. Symbols as in Fig. 8.

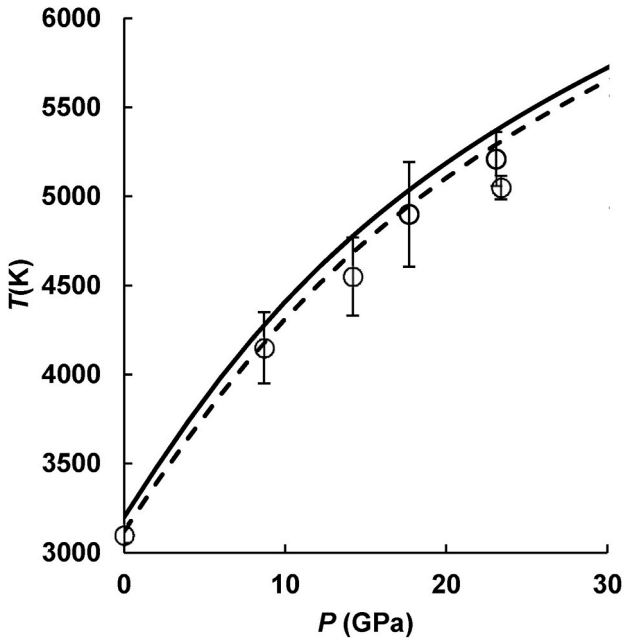

Fig. 10. MgO (periclase): *P-T* curve of melting. Solid line: quasi-harmonic model; dashed line: anharmonic model; open circles: experimental data from Ref. [43]; experimental value at room pressure by Ref. [46].

Table 2
Regression parameters of least-squares fitting and related statistical figures of merit. $T(P)$ melting functions from anharmonic model (temperature range: 3000–6000 K; number of points: 100).

Polynomial fit *		
R	1.0000	
R^2	1.0000	
adjR^2	1.0000	
MSSE	119.7077	
RMSE	0.1094	
SSE	10.9411	
MAE	0.2840	
Parameter	**Value**	**Std. Err.**
c_0	3122.4109	0.21
c_1	136.6462	0.17
c_2	−0.8769	0.05
c_3	−0.1498	0.01
c_4	7.6061E-04	6.58E-04
c_5	−1.5489E-04	6.55E-06
c_6	1.1862E-06	5.95E-08
Simon equation **		
R	0.9961	
R^2	0.9923	
adjR^2	0.9872	
MSSE	7854.3788	
RMSE	62.6673	
SSE	88.6249	
MAE	50.5539	
Parameter	**Value**	**Std. Err.**
T_0	3096.066888	.24
A	5.0936	2.49
C	3.3797	0.76

* polynomial function in P.

$T_M(P) = c_0 + c_1P + c_2P^2 + c_3P^3 + c_4P^4 + c_5P^5 + c_6P^6$

** Simon equation

$$T_M(P) = T_0 \cdot \left(\frac{P}{A}\right)^{\frac{1}{C}},$$

where: T_0 = melting temperature at room pressure; A,C = phenomenological parameters.

models near one another in the high pressure regime. This is in keeping with [48], who claim a significant reduction of the anharmonic contribution at high pressure, in many minerals. The quasi-harmonic model yields an overestimation of $T_M(P)$ of about 2.7% at room pressure (*i.e.*, T_C~3183 K, *versus* T_M 3098 K from measurements [46]), which increases by 0.19% GPa^{-1} with pressure, leading to an average disagreement of ~5.1%. The anharmonic model yields a discrepancy of about 0.5% at room pressure (T_C~3114 K), whereas the average mismatch is of ~2.9%, with an increase of disagreement of 0.14% GPa^{-1}. In general, the anharmonic correction shifts predictions closer to the experimental values with respect to the harmonic approximation.

The better ability of the anharmonic model to reproduce observations than the harmonic one is analyzed by cross-validation statistics (see Table 3), and quantified through the Normalized Residuals Squared, plotted in Fig. 11 (see Appendix for further details). Quasi-harmonic and anharmonic models near one another if we take into account the experimental uncertainties, using the following ratio: $\delta = (T_{C,theo}\text{-}T_{M,obs})/\sigma_{experimental\ uncertainty}$. Average δ-figures are 1.76 and 0.97, for quasi-harmonic and anharmonic models, respectively. This indicates that quasi-harmonic and anharmonic models provide physical descriptions that agree on average with observations within experimental uncertainties (*i.e.* deviation $< 3\sigma_{experimental\ uncertainty}$), though they still yield different trends, as discussed above. As we stated, $K_T \leq 0$, *i.e.* occurrence of a range such that at (P_C-V_C-T_C) we have $K_T = 0$, $K_T < 0$ for $V > V_C$ and $K_T > 0$ for $V < V_C$, does imply instability but does not univocally mean melting.

Yet, we believe an important contribution in elucidating the interpretation of T_C may be provided by the following aspect. In the present case, quasi-harmonic and anharmonic models yield $T_C(P)$ curves that trend close to one another. The anharmonic contribution consists in a shift, which looks like a correction, of the quasi-harmonic model that fails to provide stability leading to $K_T \leq 0$. This is associated with the implication that the atoms can no longer preserve their equilibrium positions around which they vibrate, according to either harmonic or anharmonic oscillators. Such a behavior portends an atomic migration, even predicted by the harmonic regime, though it underestimates and curbs oscillations, thus engendering a breakdown, which develops into a deep structural reconstruction, or reorganization. A different situation is observable in the case of the soft-mode driven distorsive transition from α-quartz to β-quartz. In such a case, we were not able to detect appearance of any K_T-anomaly using the quasi-harmonic approximation, though $K_T \to 0$ upon approaching the transition temperature is experimentally observable [19] and theoretically predictable by taking into account anharmonicity through a precise modelling of the anharmonic potential function and using variational calculus [49].

Eventually, it is important to point out the link between the lattice instability conditions and the Gibbs energy difference of melt *versus* solid. Let us assume that at T_0 and P_0 the solid starts melting, so that solid and melt co-exist at equilibrium. Any isobaric shift at a higher

Table 3
Statistical figures of merit to compare quasi-harmonic and anharmonic models. See Appendix about the used acronyms.

	Quasi-Harmonic model	Anharmonic model
R	0.9605	0.9840
R^2	0.9226	0.9683
MSSE	39414.9	16151.5
RMSE	171.93	110.06
SSE	198.53	127.09
MAE	246.51	166.37
F-test	71.56 (5.99)	183.27 (5.99)
KL	321.16	140.08
MLT (Crit. Val.)	3.48 (5.99)	1.18 (5.99)
PRESS	669555.4	204034.1
MEP	83694.4	25504.3
predR^2	0.7810	0.9333
AIC	86.35	79.22

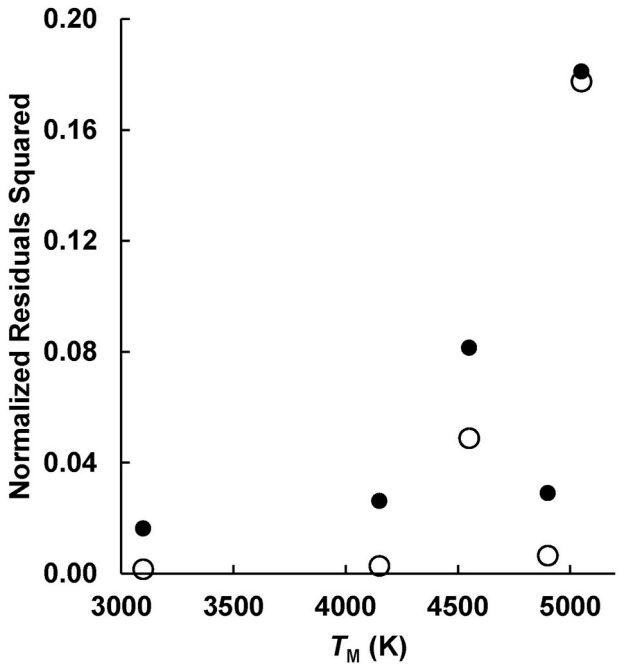

Fig. 11. MgO (periclase): Normalized residuals squared in estimating melting temperature *via* T_C. Full circles: $T_{C,theo}$ determined using the quasi-harmonic model; Empty circles: $T_{C,theo}$ determined using the anharmonic model.

temperature, $T_0+\delta T$, leads into the stability field of melt. At (P_0,$T_0+\delta T$), this implies that

$$\Delta G = \int_{T_0}^{T_0+\delta T} \left(-S(T)^{melt} + S(T)^{solid} \right) dT = \int_{T_0}^{T_0+\delta T} \Delta S(T)\, dT \; < 0,$$

and from the inequality above it descends that $\Delta S(T) < 0$. At (P_0,T_0), it holds: $S\,(T_0)^{melt} = S\,(T_0)^{solid}$.

Entropy, in turn, can be expressed by $C(T)_P$, *i.e.*

$$\Delta S(T) = \int_{T_0}^{T} \frac{-C(T')_P^{melt} + C(T')_P^{solid}}{T'} dT' \qquad (14.a)$$

From (14.*a*), it follows

$$C(T)_P^{solid} < C(T)_P^{melt}.$$

Let us recall that

$$C_P^{solid} = C_V^{solid} + \alpha^2 K_T T V, \qquad (14.b)$$

where α is the volume thermal expansion. The sign of $\alpha^2 K_T T V$ depends on K_T's. If $K_T < 0$ at $T > T_0$, then

$$C(T)_P^{solid} < C(T)_V^{solid}.$$

At very high temperature, the heat capacity at constant volume of a solid takes a flat trend and approaches its largest value, $C(T_0)_V^{solid}$. If $K(T_0)_T = 0$, therefore it ensues $C(T_0)_V^{solid} = C(T_0)_P^{solid}$. From observations [44,45], $C(T)_P^{melt}$ changes little with temperature and is larger (10–30%) than $C(T_0)_P^{solid}$. If $T > T_0$ and $K(T)_T < 0$, the following inequality must hold

$$C(T)_P^{melt} > C(T_0)_V^{solid} > C(T_0)_V^{solid} + \alpha^2 K_T T V = C(T)_P^{solid}. \qquad (15)$$

Equ.(15) shows that $K_T < 0$ is energetically associated with both thermodynamic instability and appearance of conditions entailing (14.*a*).

4. Conclusions

Melting temperature is here associated with the occurrence of the violation of fundamental thermodynamic relationships, thus causing a deep instability. We explore the case of non-positive isothermal bulk modulus, $K_T \leq 0$, predicted by both quasi-harmonic and anharmonic models. In particular, $K_T = 0$ at (P_C-V_C-T_C) signals the onset of a structural breakdown. In the case of MgO (periclase), we correlate (P_C-V_C-T_C) with melting, and detect the appearance of instability due to the occurrence of a minimum in the P–V T_C-isothermal curve, so that:

$(\partial P/\partial V)_T > 0$, $K_T < 0$, $V > V_C$, $T = T_C$

$(\partial P/\partial V)_T < 0$, $K_T > 0$, $V < V_C$, $T = T_C$,

$(\partial P/\partial V)_T = 0$, $K_T = 0$, $V = V_C$, $T = T_C$.

(P_C-V_C-T_C) is used as an estimate of melting temperature, as a function of pressure. *Ab-initio* calculations were carried out to determine lattice and vibrational components of the free energy, and hence P. Both quasi-harmonic and anharmonic models predict melting, by means of the critical points introduced above. In comparing our predictions with observations for MgO, we conclude that:

1) the quasi-harmonic model overestimates the $T_M(P)$ curve and the discrepancy between theoretical data *versus* observations increases with temperature, from ~2.7 (room pressure, experimental: ~3098 K) up to ~9% (experimental: P ~25 GPa and T ~5000 K), with an average of 5.1%;
2) the introduction of the anharmonic correction yields an agreement between calculations and experimental data within 3%, on average (at room pressure, T_C ~ 3114 K with a discrepancy ~ 0.5%);
3) quasi-harmonic and anharmonic models share similar sensitivities to pressure, in terms of mismatch between predicted *versus* observed melting temperature, the former yielding 0.19% and the latter 0.14% GPa^{-1}.

Altogether, the estimate of T_M *via* T_C is satisfactory, for periclase. Although T_C is associated with a fully established violation of fundamental thermodynamic inequalities, yet it cannot be univocally related to the occurrence of melting. However, given that such a violation is predicted by quasi-harmonic and anharmonic models alike, this suggests a deep loss of stability that implies a full structure readjustment, compatible with melting. A different case is provided by those transformations driven by soft modes that yield a relevant anharmonic contribution (for instance, α-β quartz transition) and do cause thermoelastic anomalies, which are not necessarily seen by a quasi-harmonic model. We underscore that further tests are required to provide a solid statistical basis that accounts for structural and chemical diversity between solids to substantiate the principle presented above. In particular, MgO does not present i) crystallographic degrees of freedom, other than the lattice edge, and exhibits ii) a quasi-ionic bonding. As to i), the absence of an atomic relaxation likely makes the system prone to a sharp response, in terms of loss of stability upon of heating. We reasonably expect more complex to model solids whose atoms relax along degrees of freedom, at high pressure and temperature. In this view, a further aspect that require attention is the role played by the glass transition, associated with a loss of stability of the ordered phase and whose T-range changes from substance to substance [48,49]. As to ii), we observed, in our experience, that ionic systems are better modelled than covalent ones by the computational techniques here employed. In this light, we believe efforts are to be paid to achieve a comparable degree of agreement between predictions and observations in the case of more complex bonding. All this is related to and hopefully scaled down by a progressive enhancement in the capacity of computational modelling. Notwithstanding the cautions at i) and ii), yet it is worth noting once more that $K_T < 0$ is laced with a very general condition of stability *via* Gibbs energy

in favor of a "new phase" with respect to the pristine solid one, and the failure of the harmonic model in providing stability to the original crystal structure suggests, in our opinion, to assign the "new phase" to the liquid state.

Data availability

The raw data required to reproduce these findings are available to download from https://data.mendeley.com/. The processed data required to reproduce these findings are available to download from https://data.mendeley.com/.

Declaration of competing interest

We declare that we have no conflict of interest to report.

Ackowledgements

The present study was granted by the "PRIN2017-2017L83S77" project of the Italian Ministry for Education, University and Research (MIUR). The authors are indebted with Prof. Mauro Prencipe, for useful discussions and suggestions that really improved the manuscript. The authors are grateful to two anonymous reviewers for their suggestions and corrections.

Appendix

Some cross-validation statistic markers are used for a comparison between the melting curves foreseen by quasi-harmonic and anharmonic models. Acronyms are reported below:

R = coefficient of correlation.

R^2 = coefficient of determination

$adjR^2$ = R^2 adjusted for the numbers of predictors.

MSSE = Error Mean Squared.

RMSE = Root Mean Squared Error.

SSE = Standard Error of Regression Estimates.

MAE = Mean Absolute Error.

F-test = Model F-test (» 1; the highest F is, the better the reliability of the model).

KL = Kullbak-Leibner divergence (a measure of how observations data set is different from the calculated one).

PRESS = Prediction Error Sum of Squares (The smaller PRESS is, the better the predictability of the model).

MEP = Mean Error of Prediction (The smaller MEP is, the better the predictability of the model).

MLT = Modified Levene Test for Constant Variance (must be below the Critical Value).

$predR^2$ = R^2 prediction (predictive power of the model).

AIC = Akayke Information Criteria (The best model shows the lowest value of AIC).

NRS = Normalized Residuals Squared, i.e., the residuals e_i normalized by an estimated value of their standard error $e_i/(\mathbf{e}^T\mathbf{e})^{1/2}$.

Appendix A. Supplementary data

Supplementary data to this article can be found online at https://doi.org/10.1016/j.calphad.2021.102259.

References

[1] M.M. Walz, D. van der Spoel, Systematically improved melting point prediction: a detailed physical simulation model is required, Chem. Commun. 55 (2019) 12044–12047, https://doi.org/10.1039/c9cc06177krsc.li/chemcomm.
[2] F.A. Lindemann, The calculation of molecular vibration frequencies, Phys. Z. 11 (1910) 609–612.
[3] J.J. Gilvarry, The Lindemann and grüneisen laws, Phys. Rev. 102 (1956) 308–316, https://doi.org/10.1103/PhysRev.102.317.
[4] M. Ross, Generalized Lindemann melting law, Phys. Rev. 184 (1969) 233–242, https://doi.org/10.1103/PhysRev.184.233.
[5] Y. Kuramoto, Theory of melting transition, Prog. Theor. Phys. 45 (6) (1971) 1724–1736, https://doi.org/10.1143/PTP.45.1724.
[6] F.D. Stacey, R.D. Irvine, Theory of melting: thermodynamic basis of Lindemann's law, Aust. J. Phys. 30 (1977) 631–640, https://doi.org/10.1071/PH770631.
[7] K.F. Herzfeld, M. Goeppert Mayer, On the theory of fusion, Phys. Rev. 46 (1934) 995–1001, https://doi.org/10.1103/PhysRev.46.995.
[8] M. Born, Thermodynamics of crystals and melting, J. Chem. Phys. 7 (1939) 591–603, https://doi.org/10.1063/1.1750497.ISSN0021-9606. AIP Publishing.
[9] Y. Ida, Theory of melting based on lattice instability, Phys. Rev. 187 (1969) 951–958, https://doi.org/10.1103/PhysRev.187.951.
[10] L.L. Boyer, Theory of melting based on lattice instability, Phase Transitions 5 (1985) 1–48, https://doi.org/10.1080/01411598508219144.
[11] F.J. Owens, The thermo-elastic instability model of melting of alkali halides in the Debye approximation, Phase Transitions 91 (2018) 503–508, https://doi.org/10.1080/01411594.2018.1432052.
[12] R.M. Digilov, H. Abramovich, Temperature variation of the isothermal bulk modulus in solids: thermo-elastic instability and melting, J. Appl. Phys. 125 (2019), 065104, https://doi.org/10.1063/1.5078722.
[13] A.B. Belonoshko, L.S. Dubrovinsky, Molecular dynamics of NaCl (B1 and B2) and MgO (B1) melting: two phase simulation, Am. Mineral. 81 (1996) 303–316, https://doi.org/10.2138/am-1996-3-404.
[14] L. Vočadlo, G.D. Price, The melting of MgO — computer calculations via molecular dynamics, Phys. Chem. Miner. 23 (1996) 42–49, https://doi.org/10.1007/BF00202992.
[15] P. Tangney, S. Scandolo, Melting slope of MgO from molecular dynamics and density functional theory, J. Chem. Phys. 131 (2009) 124510, https://doi.org/10.1063/1.3238548.
[16] H.B. Callen, Thermodynamics, John Wiley & Sons Inc, 1960.
[17] D.C. Wallace, Thermodynamics of Crystals, John Wiley & Sons Inc, 1972.
[18] M.A. Bouhifd, G. Gruener, B.O. Mysen, P. Richet, Premelting and calcium mobility in gehlenite (Ca2Al2SiO7) and pseudowollastonite (CaSiO3), Phys. Chem. Miner. 29 (2002) 655–662, https://doi.org/10.1007/s00269-002-0276-0.
[19] P. Richet, J. Ingrin, B.O. Mysen, P. Courtial, P. Gillet, Premelting effects in minerals: an experimental stud, Earth Planet Sci. Lett. 121 (1994) 589–600, https://doi.org/10.1016/0012-821X(94)90093-0, 3–4.
[20] R.J. Angel, · M. Alvaro, · R. Miletich, F. Nestola, A simple and generalised P–T–V EoS for continuous phase transitions, implemented in EosFit and applied to quartz, Contrib. Mineral. Petrol. 172 (2017) 1–15, https://doi.org/10.1007/s00410-017-1349-x.
[21] M. Merli, A. Pavese, Electron-density critical points analysis and catastrophe theory to forecast structure instability in periodic solids, Acta Crystallogr. A74 (2018) 102–111, https://doi.org/10.1107/S2053273317018381.
[22] T. Poston, I. Stewart, Catastrophe Theory and its Applications, Series: Dover Books on Mathematics, Dover Publications, 1996, ISBN 9780486692715.
[23] R. Lakes, K.W. Wojciechowski, Negative compressibility, negative Poisson's ratio, and stability, Phys. Status Solidi 245 (2008) 545–551, https://doi.org/10.1002/pssb.200777708.
[24] A.B. Cairns, A.L. Goodwin, Negative linear compressibility, Phys. Chem. Chem. Phys. 17 (2015) 20449–20465, https://doi.org/10.1039/C5CP00442J.
[25] A.R. Oganov, P.I. Dorogokupets, All-electron and pseudopotential study of MgO: equation of state, anharmonicity, and stability, Phys. Rev. B 67 (2003) 224110, https://doi.org/10.1103/PhysRevB.67.224110.
[26] R. Dovesi, A. Erba, R. Orlando, C.M. Zicovich-Wilson, B. Civalleri, L. Maschio, M. Rérat, S. Casassa, J. Baima, S. Salustro, B. Kirtman, Quantum-mechanical condensed matter simulations with CRYSTAL, WIREs Computational molecular science 8 4 (2018), e1360, https://doi.org/10.1002/wcms.1360.
[27] R. Dovesi, V.R. Saunders, C. Roetti, R. Orlando, C.M. Zicovich-Wilson, F. Pascale, B. Civalleri, K. Doll, N.M. Harrison, I.J. Bush, Ph D'Arco, M. Llunell, M. Causà, Y. Noël, CRYSTAL14 User's Manual, University of Torino, 2014.
[28] Z. Wu, R.E. Cohen, More accurate generalized gradient approximation for solids, Phys. Rev. B 73 (2006) 235116–235121, https://doi.org/10.1103/PhysRevB.73.235116.
[29] H.J. Monkhorst, J.D. Pack, Special points for Brillouin-zone integrations, Phys. Rev. B 13 (1976) 5188–5192, https://doi.org/10.1103/PhysRevB.13.5188.
[30] G. Gilat, L.J. Raubenheimer, Accurate numerical method for calculating frequency-distribution in solids, Phys. Rev. 144 (1966) 390–395, https://doi.org/10.1103/PhysRev.144.390.
[31] M. Causà, R. Dovesi, C. Pisani, C. Roetti, Electronic structure and stability of different crystal phases of magnesium oxide, Phys. Rev. B 33 (1986) 1308–1316, https://doi.org/10.1103/physrevb.33.1308.
[32] M. Towler, N.L. Allan, N.M. Harrison, V.R. Saunders, W.C. Mackrodt, E. Aprà, Ab initio study of MnO and NiO, Phys. Rev. B 50 (1994) 5041–5054, https://doi.org/10.1103/PhysRevB.50.5041.
[33] G. Sophia, P. Baranek, C. Sarrazin, M. Rerat, R. Dovesi, Unpublished, http://www.crystal.unito.it/index.php, 2014.
[34] M. Towler, CRYSTAL resources page. Theory of condensed matter. http://www.tcm.phy.cam.ac.uk/~mdt26/crystal.html, 2015.
[35] D.G. Anderson, Iterative procedures for nonlinear integral equations, J. Assoc. Comput. Mach. 12 (1965) 547–560, https://doi.org/10.1145/321296.321305.
[36] F. Pascale, C.M. Zicovich-Wilson, F. López Gejo, B. Civalleri, R. Orlando, R. Dovesi, The calculation of the vibrational frequencies of crystalline compounds and its implementation in the CRYSTAL code, Comput. Chem. 25 (2003) 888–897, https://doi.org/10.1002/jcc.20019.

[37] M. Rang, G. Kresse, First-principle study of the melting temperature of MgO, Phys. Rev. B 99 (2019) 184103, https://doi.org/10.1103/PhysRevB.99.184103.
[38] MATLAB, The MathWorks, Inc., Natick, Massachusetts, United States, 2019.
[39] G. Fiquet, P. Richet, G. Montagnac, High-temperature thermal expansion of lime, periclase, corundum and spinel, Phys. Chem. Miner. 27 (1999) 103–111, https://doi.org/10.1007/s002690050246.
[40] Y. Fei, Effect of temperature and composition on the bulk modulus of (Mg,Fe)O, Am. Mineral. 84 (1999) 272–276, https://doi.org/10.2138/am-1999-0308.
[41] Z. Wu, R.M. Wentzcovitch, K. Umemoto, B. Li, K. Hirose, J.-C. Zheng, Pressure-volume-temperature relations in MgO: an ultrahigh pressure-temperature scale for planetary sciences applications, J. Geophys. Res. 113 (2008) B06204. https://10.1029/2007JB005275.
[42] M. Merli, L. Sciascia, A. Pavese, V. Diella, Modelling of thermo-chemical properties over the sub-solidus MgO–FeO binary, as a function of iron spin configuration, composition and temperature, Phys. Chem. Miner. 42 (2015) 347–362, https://doi.org/10.1007/s00269-014-0725-6.
[43] T. Kimura, H. Ohfuji, M. Nishi, T. Irifune, Melting temperatures of MgO under high pressure by micro-texture analysis, Nat. Commun. 8 (2017) 15735, https://doi.org/10.1038/ncomms15735.
[44] P. Richet, Y. Botting, Anorthite, andesine, wollastonite, diopside, cordierite and pyrope: thermodynamics of melting, glass transitions, and properties of the amorphous phases, Earth Planet Sci. Lett. 67 (1984) 415–432, https://doi.org/10.1016/0012-821X(84)90179-1, 1984.
[45] T.J.B. Holland, R. Powell, An internally consistent thermodynamic data set for phases of petrological interest, J. Metamorph. Geol. 16 (1998) 309–343, https://doi.org/10.1111/j.1525-1314.1998.00140, 1998.
[46] L. Dubrovinsky, S. Saxena, Thermal expansion of periclase (MgO) and tungsten (W) to melting temperatures, Phys. Chem. Miner. 24 (1997) 547–550, https://doi.org/10.1007/s002690050070.
[47] N. de Koker, L. Stixrude, Self-consistent thermodynamic description of silicate liquids, with application to shock melting of MgO periclase and MgSiO3 perovskite, Geophys. J. Int. 178 (2009) 162–179, https://doi.org/10.1111/j.1365-246X.2009.04142.x.
[48] M. Prencipe, Role of Anharmonicity in α→β Quartz Phase Transition, Personal Communication, 2020.
[49]] F.D. Stacey, D.G. Isaak, Anharmonicity in mineral physics: a physical interpretation, J. Geophys. Res. 108 B9 (2003) 2440–2444, https://doi.org/10.1029/2002JB002316.